36th AIAA Thermophysics Conference
23-26 June 2003, Orlando, Florida

AIAA-2003-3898

Combined Laser Absorption Spectroscopy and Probe Measurements in Inductively Heated High Enthalpy Plasmas

Makoto Matsui[1], Georg Herdrich[2], Monika Auweter-Kurtz[3] , and Kimya Komurasaki[4]

[1,4]Department of Advanced Energy, University of Tokyo,
Hongo 7-3-1, Bunkyo, Tokyo 113-0033, Japan

[2,3]Institut für Raumfahrtsysteme (IRS), Universität Stuttgart
Pfaffenwaldring 31, D-70550 Stuttgart, Germany

Keywords: inductive plasma generator, laser absorption spectroscopy

Abstract

The production of high enthalpy flows in a stationary manner requires plasma wind tunnels using plasma generators. Magnetoplasmadynamic generators (MPG), thermal arcjet devices (TPG) and inductively heated plasma generators (IPG) have been developed at the IRS for different atmospheres, different atmospheric entry regimes and/or different basic investigations.

The absence of electrodes enables the use of IPGs for basic TPS material tests (e.g. catalycity) and the simulation of re-active atmospheres such as the Martian or Venerian atmosphere.

With IPG3 an rf-source is provided where the coil is closer to the plasma than it was with previous designs. Therefore, the electromagnetic field loss is reduced. The water cooling system surrounds both the induction coil and the plasma container. This paper describes the design of IPG3 and the experimental results using O_2. Three test cases with pure O_2 plasma were investigated using the absorption spectroscopy system of Department of Advanced Energy, the University of Tokyo, in combination with a Pitot pressure probe and a material sample support system of IRS, Universität Stuttgart. Number density and translational temperature distributions of atomic oxygen were obtained from the measured absorption line profiles including absorption lines of meta-stable atomic oxygen at 777.19 and excited atomic oxygen at 844.64 nm. Mach number was deduced by the ratio between pitot pressure and ambient pressure. Surface temperature of TPS materials was measured by thermocouplers.

[1]Graduate student, Student Member AIAA
[2]Research engineer
[3]Professor, Senior Member AIAA
[4]Associate Professor, Senior Member AIAA

1. Introduction

A variety of stringent requirements upon technology are imposed by both space travel to a rather close Earth orbit and to more distant celestial bodies such as the planets of our solar system. Among those requirements there are the high temperature effects occurring during atmospheric entries. Here, spacecrafts encounter gases at velocities of more than ten km/s, thereby being subjected to great heat loads. This makes it necessary to use high temperature thermal protection systems (TPS) to prevent the destruction of the space vehicle. Both TPS and environment (plasma) during the entry have to be investigated by means of computational and ground facility based simulations. Such ground facilities are the five IRS plasma wind tunnels PWK1-5 that reproduce the thermal, aerodynamic and chemical load on the surface of a space vehicle entering a celestial body's atmosphere.

MPGs enable gas flows on high enthalpy levels. They are mainly used to investigate the erosion of radiation-cooled heat shield materials like C-C or C-SiC as well as the behavior of ablative materials under thermal and chemical loads. Two IRS plasma wind tunnels are operated with MPGs. Furthermore, a TPG producing moderate enthalpies and higher stagnation pressures to simulate the follow on flight path is in use [1, 2].

As an IPG is contactlessly heated by induction currents, exceptionally pure plasma flows of any gases can be produced. Therefore, the application of an IPG delivers two major advantages. First, researchers are aware that the catalytic behavior of TPS materials is one of the main topics to be investigated in future. A main part of the heat flux seen by a TPS material derives from the recombination of atomic plasma species. Using the IPG the related heat flux measurements are not falsified by impurities as with the electrode plasma generators. Furthermore, the catalytic mechanisms of single gases such as of O_2 and N_2 [3, 4] in the case of air of an atmosphere can be investigated. Fig. 1 shows a typical pure oxygen plasma plume of IPG3 at 500Pa ambient pressure, an oxygen mass flow rate 3g/s and at an anode voltage U_A=6250V. The resonant circuit was adjusted to nominal 650kHz using a 5-turn coil with 7 capacitors each of 6nF (see description below).

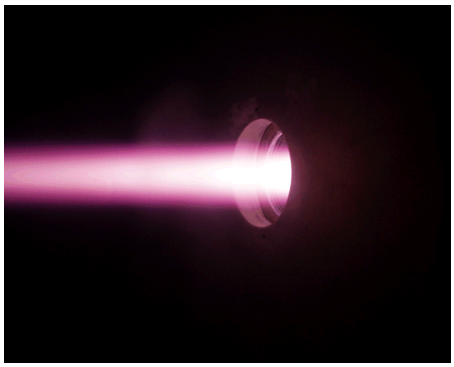

Fig. 1 IPG3 Oxygen plasma plume at ambient pressure of 500Pa (anode power 105kW)

In addition, applications in the range of plasma diagnostics on ground and in situ (flight experiments) such as heat flux measurements using materials with different, but well-known catalycities can be performed. Here, it is possible to determine the atomic species concentrations within the plasma [5,6]. For the direct investigation of the plasma wind tunnel plume's composition, a quantitative and non-intrusive measurement is feasible. Such powerful nonintrusive measurement techniques and methods like emission spectroscopy, laser induced fluorescence (LIF) and Fabry-Perot interferometry (FPI) are used at IRS to investigate the plasma flows [7]. They are used to determine atomic and molecular density and the velocity distribution in the boundary layer. Furthermore a diode-laser absorption spectroscopy (LAS) technique [8] of the University of Tokyo was used for IRS-PWK3. This portable system is a very suitable measurement technique for the measurement of number densities and translational temperatures e.g. of O_2 [9]. The LAS is able to access absorbing atoms and molecules even in high temperature and/or high Mach number flows [8].

The second advantage of IPGs is to be seen in the possibility of performing re-entry simulations for celestial bodies like Mars or Venus, where there are rather reactive gas components such as CO_2. Here, the IRS has already performed high enthalpy CO_2 tests that showed that PWK3-IPG3 is able to perform re-entry simulations for atmospheres containing CO_2 [3]. A nozzle equipped inductively heated plasma generator IPG4 was developed and tested. This device enables the operation with CO_2 at higher total pressures while rather low mass flow rates are required. Additionally, a procedure deactivates the explosive CO_2-Plasma using N_2 as deactivator [10]. This enables participation in campaigns such as "Venus sample return missions" or "Mars Mini-Probes" that are presently under investigation by ESA [11, 12, 13].

Mass spectrometry, electrostatic and radiation probes also belong to the group of intrusive measurement techniques. As the name already suggests, this diagnostic method is based on a suitably constructed probe being mounted in the plasma stream, which is to be investigated. The mechanical probes are among the most important instruments for plasma diagnostic measurements and are therefore often used. Besides the standard sample support system which carries the TPS material sample to be tested, Pitot pressure probes, aerodynamic wedge probes (Mach number determination), heat flux probes, enthalpy probes and solid state electrolyte probes for determining the oxygen particle pressure are used to characterize the plasma. All of these probes can be installed at the IRS on moveable platforms inside the plasma wind tunnels. Electrostatic probes are used to ascertain the plasma potential, electron density and temperature, energy distribution of the electrons, ion temperature, flow velocity and direction. The measurement principle is based on an active influence on the plasma boundary layer which forms on the probe. The use of radiometric probes is unavoidable when the radiation heat flux can not be neglected compared to the convective part. This is the case when during sample return missions the entry speed into the Earth's atmosphere is especially high or when the atmosphere of another celestial body (that is to be entered) contains strong radiating species, as for example the atmosphere of Titan. A general overview for the IRS plasma diagnostic tools is given in [7].

2. Set-up of PWK3 and the IPG

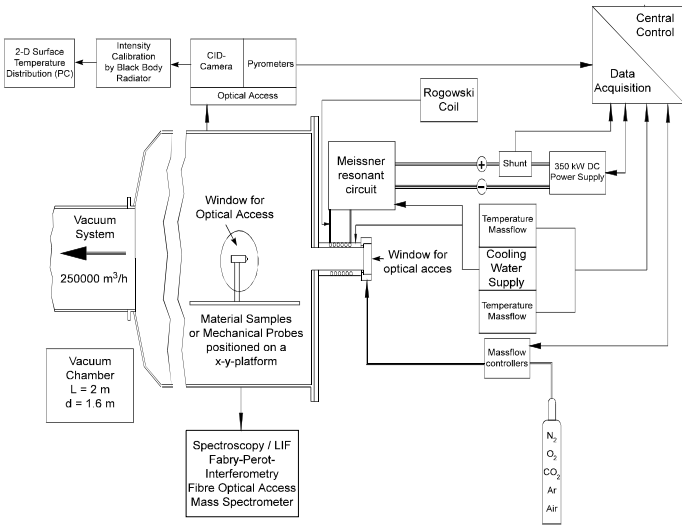

Fig. 2 Scheme of plasma wind tunnel PWK3

The general facility set-up shown in Fig. 2 consists of the IPG plasma source and the vacuum chamber. Its size is about 2m in length and 1.6m in diameter. Optical accesses to the vacuum chamber enable the measurement of the plasma. A heat exchanger between the test chamber and the vacuum system cools down the hot plasma to protect the vacuum system from being damaged. The plain lid of PWK3 (left side of chamber, see Fig.2) carries the IPG and the external resonant circuit that consists of the capacitors with the connection to the plasma generator. The right side flange of the vacuum chamber is connected to the IRS vacuum pump system. It is used to simulate pressures at

altitudes up to 90 km. The system consists of four stages: the first two stages are roots blowers, the third stage is a multiple slide valve type pump, and the last stage (pumping up to atmospheric pressure) is a rotary vane type pump. Total suction power of the pumps amounts to 6.000m^3/h at atmospheric pressure and reaches about 250.000m^3/h at 10Pa measured at the intake pipe of the system, which has a diameter of 1m. The base pressure of the system is 0.5Pa. The desired tank pressure can be adjusted between the best achievable vacuum and 100kPa by removing one or more pumps from the circuit and/or mixing additional air into the system close to the pumps.

The external resonant circuit is cooled by a water-cooling circuit. With this the capacitors, which have a capacity of 6000pF ±20% each, and the inductor are cooled. The resonant circuit is built in Meissner type switching [14] using a metal ceramic triode with an oscillator efficiency of about 75% [15] (see Fig. 3).

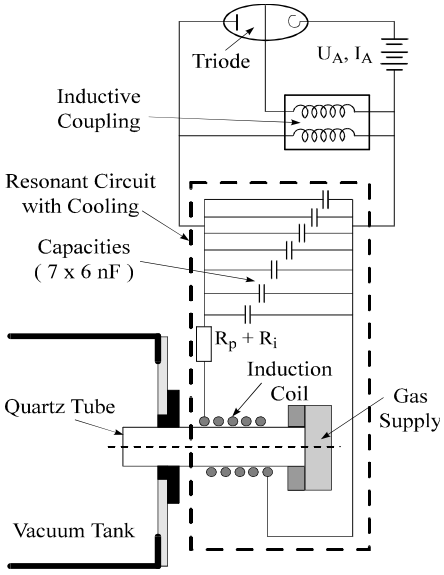

Fig. 3 Scheme of the PWK3 Meissner type resonant circuit

Its nominal frequency can be changed by switching the order or number of capacitors (see Fig.3) as well as by the use of coils with different inductivities. The error bars in Fig.4, which shows the 7 different nominal frequencies, take into account the tolerances of the capacitors [14].

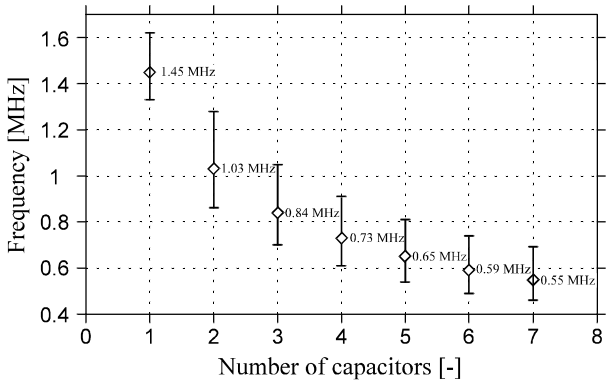

Fig. 4 Nominal operating frequencies for different capacitor switchings, $L_{inductor}$=2µH (see text)

For the present investigations the frequency has been tuned to the nominal frequencies of 0.74MHz (4 capacitors) using a water-cooled 5-turn coil with a length of about 120mm. This coil geometry leads to an inductivity of about 2µH. The whole circuit is switched to a 375kW power supply. The incoming anode power can be adjusted by the control of the anode voltage.

Inductively heated plasma generators basically consist of an induction coil surrounding a plasma container (tube) and capacities, as schematically shown in Fig.3. This resonant circuit is fed by an energy supply. The alternating current in the coil induces a mostly azimuthal electric field inside the tube. This electric field initiates an electric discharge in the gas that is injected at one side into the tube (see Fig.5). The produced plasma is expanded into the vacuum chamber. The electric discharge in the plasma is carried by mostly azimuthal eddy currents. The current amplitude and thus the Ohmic heating strongly depends on the electric conductivity of the plasma and the resonant frequency.

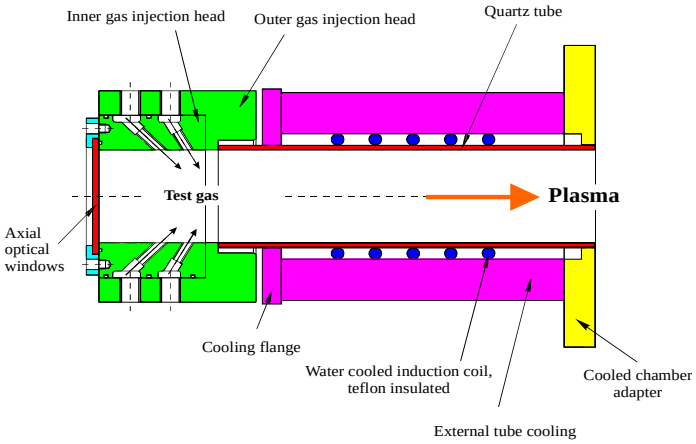

Fig. 5 View of the plasma source IPG3

The principal parts of the plasma generator IPG3 are described here. An axial optical access through the inner

injection head enables investigations of the plasma inside the generator (see Fig. 5). The tube cooling system is transparent; therefore, the position of the "plasma flame" within the tube can be observed with regard to different operating parameters such as chamber pressure, gas, mass flow and anode power. Additionally, this feature is supported by the axial optical window. The total length of IPG3 is about 0.35m, its diameter about 0.1m.

The quartz tube contains the produced plasma which leaves the generator through the water-cooled chamber adapter. The induction coil is connected to the external resonant circuit (Figs.2,3) delivering power and cooling water for IPG3. Furthermore, both the tube and the coil are surrounded by the external tube cooling, which protects the quartz tube from overheating. The water and an additional cage around the generator serve as an rf-radiation protection shield.

3. Measurement Techniques

A variety of probes and optical diagnostic techniques that have been developed and qualified at the IRS has been surveyed in the introduction of this paper. Precise descriptions have been made in [7]. The LAS measurement technique developed at the University of Tokyo, is a modularly built system enabling a quite simple installation. Additionally, its sub-system is rather small such that a transport of the system from Japan to Germany was feasible. A precise description of the system is given in [9]. In the section below, the measurement techniques that have been used for the measurements presented in this paper are described.

3. 1 Operational Parameter of PWK3-IPG3

The Meissner type resonant circuit is supplied by the DC anode power P_A measured during the operation of the device [2, 3, 10, 16]. The anode voltage U_A is controlled. Hence, the anode current I_A results from the load of the resonant circuit (plasma) and the accompanying operating conditions. Thermal powers such as tube cooling power and resonant circuit power are measured using resistance thermometers. They are electrically sealed and installed at an acceptable distance from the plasma source in order to prevent disturbing signals from the rf-field. Additionally, the cooling water flow rates are measured. A cavity calorimeter was developed to measure the thermal plasma power [2]. However, this exceeded the time schedule of the performed measurement campaign. It is intended to perform such a measurement in a later campaign.

Mass flow of the test gas and the pressure of the inner gas injection head are measured as well. A modified Pearson current monitor can be used to determine the operational frequencies [17].

3.2 Probe Measurements

The Pitot probe (Fig.6) used for this investigation is geometrically similar to the material support system, which was used for material tests. Both belong to the IRS probe set developed within the Hermes program and the Special research Center 259. Their geometries i.e. the outer diameter of 50mm and the corresponding cupon material sample diameter of 26.5mm became the so-called European standard geometry.

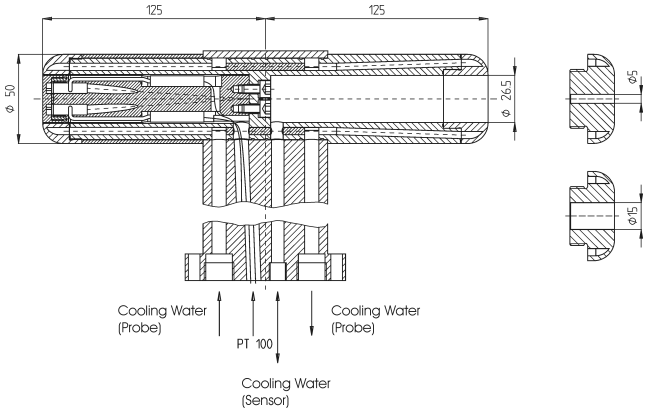

Fig. 6 Pitot probe (European standard geometry)

3.3 Principe of Laser Absorption Spectroscopy (LAS)

There are two major advantages in LAS method. It can be applicable even to optically thick plasmas and it does not require the absolute absorption quantity but the fractional one. Number density of the particles in absorption levels and translational temperature are available, as follows.

Number density The relationship between laser intensity I_ν, and absorption coefficient k_ν in a substance is expressed as,

$$\ln \frac{I_\nu}{I_{\nu 0}} = -\int k_\nu dx \tag{1}$$

Here, $I_{\nu 0}$ I_ν, ν are incident laser intensity, transmitted laser intensity, and laser frequency, respectively. Assuming axisymmetric distributions, the local k_ν is obtained by the Abel inversion.

Although measured k_ν is a sum of absorption and stimulated emission coefficients, stimulated emission is neglected. Then, the relationship between integrated absorption coefficient $K(r)$ and population density at the absorbing state n_i is given as

$$K(r) = \int k_\nu \mathrm{d}\nu = \frac{\lambda^2}{8\pi} \frac{g_j}{g_i} A_{ji} n_i \tag{2}$$

Here, λ is the wavelength, i, j are lower and upper energy levels, A_{ji} is the Einstein's emission coefficient, g_i and g_j are statistical weights.

Translational temperature Generally, an absorption profile is broadened by various physical mechanisms.

Doppler broadening is the statistical one originating from thermal motion of the particle. The profile is Gauss type and the full width at the half maximum $\Delta\nu_D$ is expressed as,

$$\Delta\nu_D = \frac{\sqrt{8R\ln 2}}{\lambda_0}\sqrt{\frac{T}{M}} \tag{3}$$

Here, c is the velocity of light, R is gas constant, λ_0 is the center frequency of the absorption, M is the atomic weight of the absorbing atom and T is the translational temperature.

Other broadenings such as natural, pressure and stark ones are all Lorentz type and are much smaller than Doppler one in our experimental conditions.

Absorption Lines In this study, three absorption line of atomic oxygen were targeted. 777.19nm line is absorption from the meta-stable state (3s5S) and 844.64nm are absorption from the state (3s3S), which is connected to the ground level by radiative transitions. The transition data of these lines is listed in Table 1 and the energy level diagram is shown in Fig. 7.

Table 1 Transition data

i	j	λ(nm)	E_i (eV)	E_j (eV)	g_i	g_j	A_{ji} ($10^7 s^{-1}$)
$3s^5S$	$3p^5P$	777.19	9.14	10.7	5	7	3.69
$3s^3S$	$3p^3P$	844.62	9.52	11.0	3	1	3.22
$3s^3S$	$3p^3P$	844.64	9.52	11.0	3	5	3.22

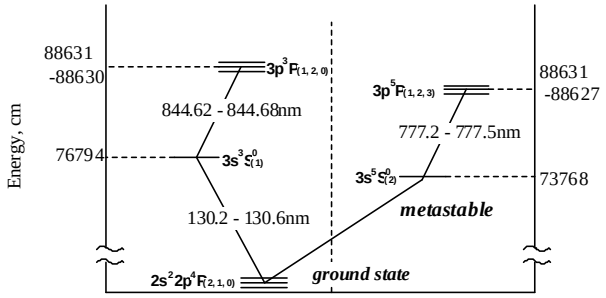

Fig. 7 Energy level diagram

3.4 Experimental setup for LAS

The system's laser source is a tunable diode laser with an external cavity (Velocity Model 6300, New Focus, Inc.). It guarantees minimum mode hopping during the oscillation-frequency modulation. The line-width of the laser is as small as 500 kHz. An optical isolator is used to prevent the reflected laser beam from returning into the external cavity. A Fabry-Perot etalon with a free spectral range of 1 GHz is used to provide reference frequency spacing. The laser beam was introduced into a test chamber through an optical fiber. All the laser and measurement systems are transported from Japan to Germany because they are very compact and portable.

Figure 8 shows the set-up of the LAS together with PWK3. The laser was introduced through the right side optical flange of PWK3. The laser collimator was fixed onto the optical window using a movable stage with a step motor in between. This enabled the measurement of radial absorption profiles. The detector was put on the left side flange. The minimal detectable distance from the generators outlet (see Fig. 1) was 130mm due to the position of the right side window.

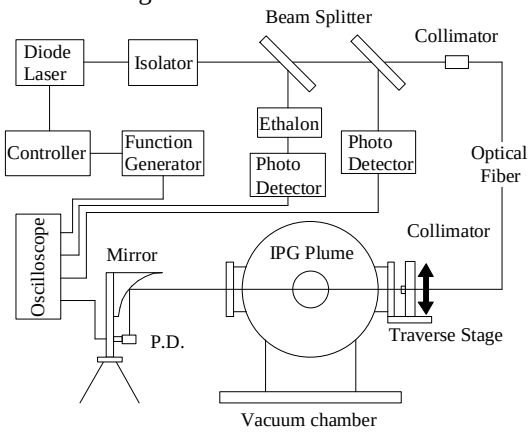

Fig.8 Optical system

5. Results

5.1 Test conditions

All the tests were performed with pure oxygen plasma using four capacitors with a 2μH coil (f = 0.74 MHz). Three different cases were tested:

Case 1a: Ambient pressure is 500Pa, oxygen mass flow rate 3g/s, anode voltage 6250V and anode power 106kW. At this ambient pressure, the plume is not expanding and the plume diameter is almost the same as the heater exit at 393mm downstream. A photograph of IPG3 with this condition is shown in Fig. 1.

Case 1b: A probe (Pitot pressure probe) is inserted in the plume and the region in front of the probe (Pitot pressure probe) is measured. The operating conditions are the same as **case 1a**. Strong illumination region is limited to the very vicinity of the probe so that density profile could be obtained for the condition. Unfortunately, only information from the preliminary data was available for this condition.

Case 2a: The ambient pressure is 50Pa (i.e. facility base pressure), the oxygen mass flow rate4 g/s, the anode voltage 6060V and the anode power 83kW. This condition is also known as the so-called FESTIP* condition. The measurement point is also at 393mm downstream distance from the IPG exit.

Case 2b: Material sample holder system or Pitot probe are inserted. The operating conditions are the same as **case 2a**.

Case 3 The ambient pressure is 30Pa the oxygen mass flow rate 4~6 g/s, the anode voltage 6250V and the anode power 110kW. The measurement plane is 130mm from the IPG exit.

5.2 Experimental results using the Pitot probe and the material support system

* Future European Space Transport Investigation Program; this plasma generator condition was used for SSiC material tests within the program.

Table 2 summarizes the conditions measured with the probes. Mach numbers were calculated one-dimensionally using the calculated ratio P_{pitot}/P_{amb}. For the sub-sonic case the Mach number can be estimated using

$$1+\frac{\kappa-1}{2}M_{a1}^2=\left(\frac{p_{tot}}{p_{amb}}\right)^{\frac{\kappa-1}{\kappa}} \quad . \tag{4}$$

For the supersonic case we have to use

$$\frac{\frac{\kappa+1}{2}M_{a1}^2}{\left(\frac{2\kappa}{\kappa+1}M_{a1}^2-\frac{\kappa-1}{\kappa+1}\right)^{\frac{1}{\kappa}}}=\left(\frac{p_{tot}}{p_{amb}}\right)^{\frac{\kappa-1}{\kappa}}, \tag{5}$$

where κ is the specific heat ratio and M_{a1} is the Mach number. Both equations assume constant heat capacities. Static pressure is assumed to be identical to the ambient pressure in the vacuum chamber. Hence, measured pressure ratio leads to Mach number in the form

$$Ma = f\left(p_{Pitot}/p_{amb},\kappa\right). \tag{6}$$

In Fig. 9 the resulting Mach numbers are illustrated. The full symbols show the interval calculated using Eq. (4), while the empty symbols were calculated with Eq. (5).

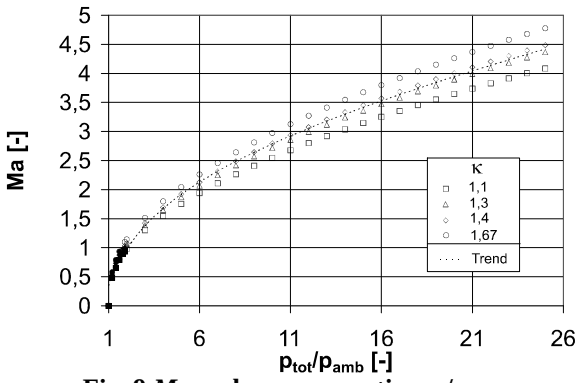

Fig. 9 *M*a and pressure ratio p_{tot}/p_{amb}

The resulting values for the test cases are presented in Table 2.

Table 2 Measured P_{Pitot}, T_{wall}, estimated *M*

Case	P_A [kW]	P_{pitot} [Pa]	P_{pitot}/P_{amb}	T_{Wall} [°C]	Mach
1a	106	950	1.9	-	1.05
1b	106	950	1.9	1210	1.05
2a	83	190	3.8	-	1.6
2b	83	190	3.8	1050	1.6

For case 1b a material test using SSiC was performed (see Fig 10). This enables an estimative determination of the heat flux under this condition which is about 230kW/m^2. During the test the ambient pressure was increased as shown in Fig. 10. The pressure control system was worked over the 500Pa threshold (above 600Pa, thin black curve) which can be seen as temperature effect on the material sample as well. In fact, the temperature increases up to 1250C and decreases with the reach of the 500Pa ambient pressure at t>=750s (thick gray line).

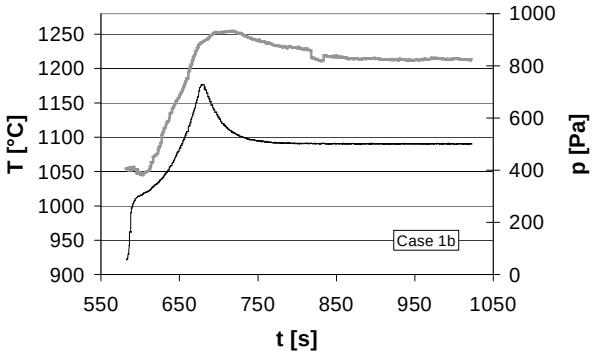

Fig. 10 Sample temperature and ambient pressure histories during the material test, x=393mm, p_{Pitot}=950 Pa (case 1b)

In Fig. 11, anode voltage U_A was plotted in the same time range as Fig. 10. However, it is visible that the voltage has already been constant at t=650 s which implies that the temperature increase seen in Fig. 10 is due to a pressure effect.

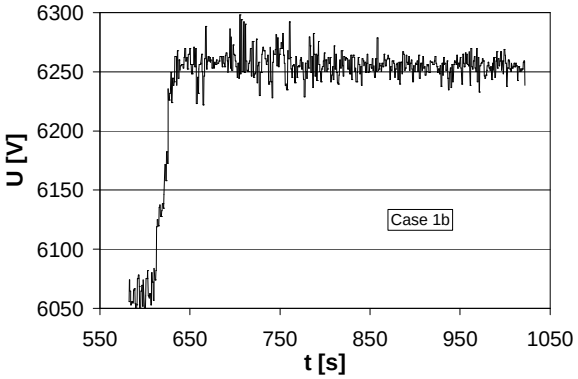

Fig. 11 anode voltage history during the material test, x=393mm, p_{Pitot}=950 Pa (case 1b)

Figure 12 depicts the Pitot pressure profile for case 2. The small, filled symbols mark the Pitot pressure while the large, empty symbols show the pressure ratio. The right side data points at about 400 mm show the measured Pitot pressures (this investigation). Additionally, the left side curves are shown from a former investigation. It can be seen that the whole condition is a super-sonic condition at rather high Mach numbers (compare Fig. 9).

Figure 13 shows the history of the SSiC sample wall temperature for case 2b. Both the Pitot pressure and the temperature are in good agreement with the FESTIP condition measured at x=130 mm where a temperature of 1360 °C and a Pitot pressure of 340 Pa were reached (not reported in this paper).

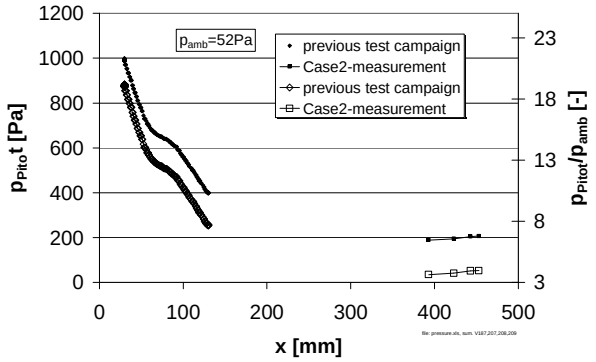

Fig. 12 Pitot pressure profile for case 2, the considered condition is at x=393 mm

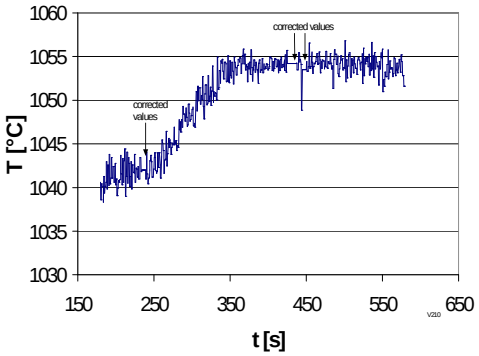

Fig. 13 Sample temperature history during the material test, x=393mm, p_{Pitot}=180 Pa (case 2b)

5.3 Experimental results using LAS

777.19nm absorption profile A typical absorption profile is shown in Fig.13 along with an etalon signal. In the IPG plasma, both emission and absorption signals fluctuated at 300Hz because of the rf-power fluctuation. Therefore, temperature is also thought fluctuating at the same frequency. In this study, temperature is defined by the envelope curve of strongest absorption in each fluctuation as a maximum one. The normalized absorption profile and the curve fit are shown in Fig.15.

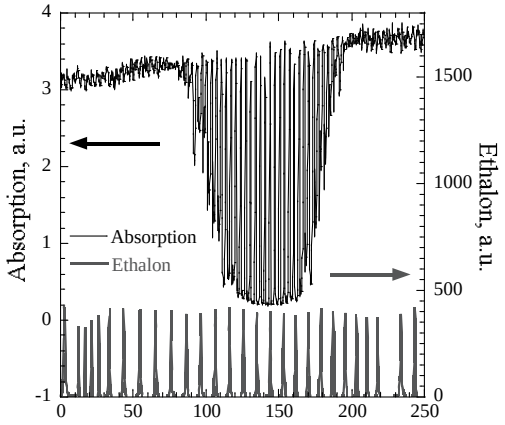

Fig.14 Typical absorption profile at 777.19nm and ethalon signal

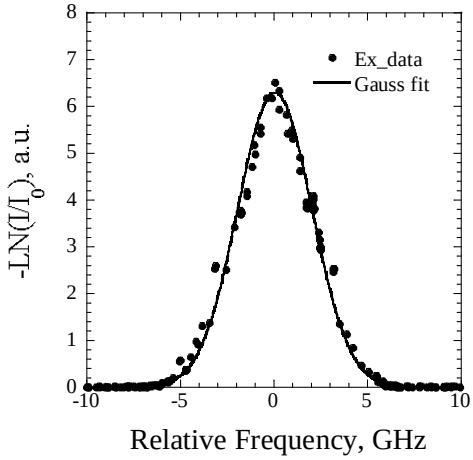

Fig.15 Maximum absorption profile (777.19 nm line) and curve fitting

844.64nm absorption profile Typical absorption profiles at 844.64nm is shown in Fig.16. The normalization method in these profiles is the same as that in 777.19 nm profiles. However, the distance between two absorption peaks (844.62 nm 844.64 nm) is very close as shown in Table1 and the profiles are superposed. Then, the profiles were fitted by two Gauss distributions with the fixed peak distance. The normalized profile and the curve fits are shown in Fig.17.

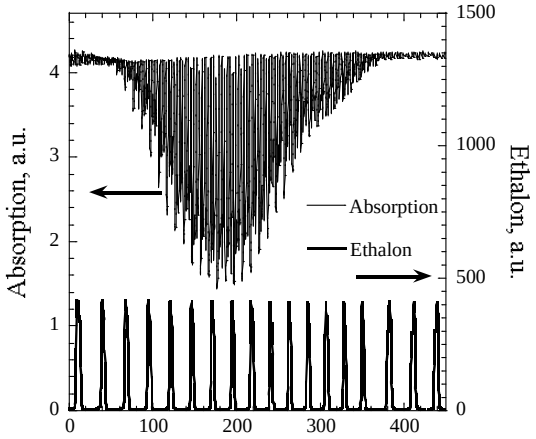

Fig.16 Typical absorption profiles at 844 nm and ethalon signal

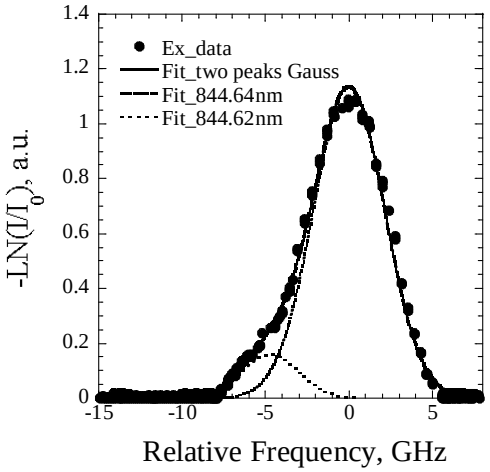

Fig.17 Maximum absorption profile (844.62, 844.64 nm line) and two peaks curve fitting

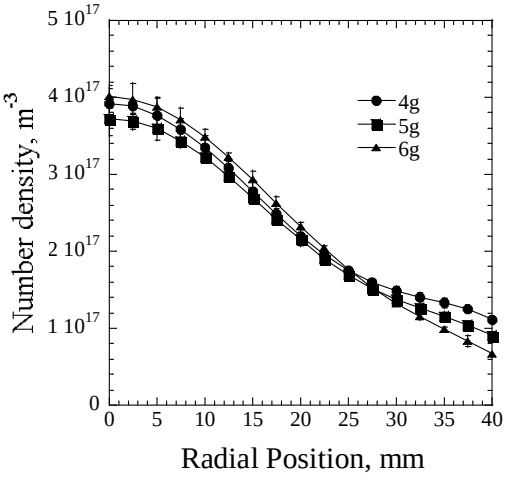

Fig.19 Number density distributions of $3s^5S$ state (meta-stable state) for various mass flow rates

Number density and Temperature distributions

The distributions of $3s^5S$ state (meta-stable state) number density and translational temperature are deduced from 777.19 nm profiles for different mass flow rate (case 3) as shown in Figs.18, 19. Translational temperature was ranged from 7,000K to 8,000K on the centerline and 4000K at the edge of the plume. Number density was $4 \cdot 10^{17} m^{-3}$ on the centerline and decreased by half at 22mm off centerline. The dependency on mass flow rates was found small in this range of mass flow rates.

Figure 20 shows the number density distributions of $3s^3S$ state under case 3 condition. The number density was $1.8 \cdot 10^{16} m^{-3}$ on the centerline and decreased by half at 22mm off centerline..

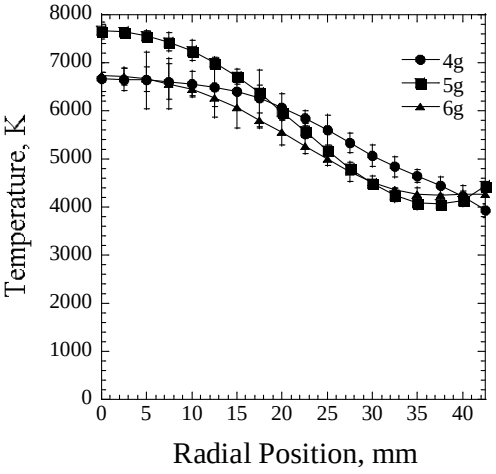

Fig.18 Translational temperature distributions for various mass flow rates

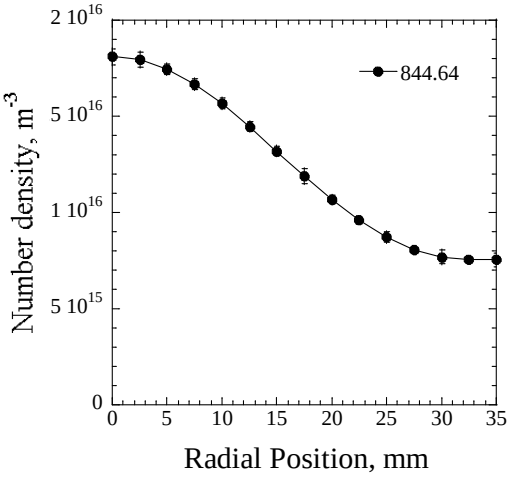

Fig.20 Number density distributions of $3s^3S$ state. $\dot{m}$ =6g/s

The oxygen is supposed to be perfectly dissociated on the centerline because of its high translational temperature. Atomic oxygen number density, which is almost equal to the ground level number density, was estimated at $1 \cdot 10^{22} m^{-3}$ from the equation of state. Then, population temperature defined by the ground state and $3s^3S$ state densities becomes 8000K, which was very close to the translational temperature. Therefore, the plume on the centerline was expected in thermal equilibrium, and also optically thick enough to be in partial Local Thermal Equilibrium.

Population of $3s^5S$ state was, unfortunately, one order of magnitude higher than p-LTE population because there is no chance of radiative depopulation.

6. Summary

Two test conditions with pure Oxygen plasmas were investigated in the inductively heated facility PWK3 using the plasma generator IPG3. For Case 1a at an ambient pressure of 500Pa, an oxygen mass flow rate 3g/s, an anode

voltage 6250V and an anode power 106kW it could be determined that the jet is less expanding than in the low presssure case. The Pitot pressure measured with the probe was 950Pa. From the one-dimensional calculation using the tank pressure as ambient pressure a Mach number slightly above 1 can be derived. The similarity of the densities for both cases 1a and 1b confirms that the shock is very week or supports that the flow Mach number is about 1. Correspondingly, a SSiC material test was performed at the same condition. Here, SSiC temperatures of 1210°C were measured leading to a partial catalytic heat flux of about 230kW/m^2. The overal simulation point "case 1" can therefore be considered as quite well known. In order to discuss about the relationship between free stream temperature/enthalpy and heat flux to the probe, CFD assuming the surface catalysis has to be used in future.

In case 2a, ambient pressure is 50Pa, oxygen mass flow rate is4 g/s, anode voltage 6060V and anode power 83kW. The condition is also known as the so-called FESTIP condition. However, the FESTIP condition is at a position of 130mm from the generator's outlet. Pitot pressure and wall temperature on SSiC were measured as well (case 2b). Pitot pressure was about 180Pa while temperature was at 1055°C.

In case 3, ambient pressure is 30Pa, oxygen mass flow rate is 4~6 g/s, anode voltage 6250V and anode power 110kW. The number density distributions of meta-stable atomic oxygen and translational temperature for different mass flow rate (case 3) deduced from 777.19 nm profiles are obtained. The translational temperature is ranged from 7,000K to 8,000K on the centerline and 4,000K at the edge of the plume. The number density is $4 \cdot 10^{17} m^{-3}$ on the centerline and decreased by half at 22mm off centerline. The dependency on mass flow rates was found small in this range of mass flow rates.

The population temperature obtained from the $3s^3S$ state density was very close to the translational temperature on the centerline. Therefore, the plume was expected in thermal equilibrium, and also optically thick enough to be in Local Thermal Equilibrium on the centerline.

References

1. M. Auweter-Kurtz, H. L. Kurtz, S. Laure, "Plasma Generators for Re-entry Simulation", Journal of Propulsion and Power, Vol. 12, No. 6, Nov./Dez. 1996.

2. M. Auweter-Kurtz, M. Feigl, M. Winter: "Overview of IRS Plasma Wind Tunnel Facilities", Paper presented on the RTO AVT Course on "Measurement Techniques for High Enthalpy and Plasma Flows", Rhode-Saint-Genèse, Belgium, published in RTO EN-8, 25-29 October 1999.

3. G. Herdrich, M. Auweter-Kurtz, H. Kurtz, T. Laux, M. Winter: Operational Behavior of the Inductively Heated Plasma Source IPG3 for Re-entry Simulations, AIAA-99-3497, 33rd Thermophysics Conference, Norfolk, VA, June 1999.

4. Laux, T, Herdrich, G., Auweter-Kurtz, M.: "Material and Heat Flux Tests with Sintered Silicon Carbide in Oxygen and Nitrogen Plasmas", Proceedings of the „First Joint French-German Symposium on Simulation of Atmospheric Entries by Means of Ground Test Facilities, Paper 3.3, University of Stuttgart, Space Systems Institute, Nov. 1999.

5. T. Stöckle, M. Auweter-Kurtz, S. Laure, "Material Catalysis in High Enthalpy Air Flows", AIAA-96-1904, 31st AIAA Thermophysics Conference, New Orleans, LA, 1996.

6. G. Herdrich, M. Auweter-Kurtz, M. Hartling, T. Laux, "Present Design of the Pyrometric Sensor System PYREX-KAT38 for X-38", International Symposium on Atmospheric Reentry Vehicles and Systems, Arcachon, France, March 1999

7. M. Auweter-Kurtz, M. Feigl, M. Winter: "Diagnostic Tools for Plasma Wind Tunnels and Re-entry Vehicles at the IRS", Paper presented on the RTO AVT Course on "Measurement Techniques for High Enthalpy and Plasma Flows", Rhode-Saint-Genèse, Belgium, published in RTO EN-8, 25-29 October 1999.

8. F.-Y. Zhang, K. Komurasaki, T. Iida, T. Fujiwara: "Diagnostics of an Argon Arcjet Plume with a Diode Laser", Journal of Appplied Optics, Vol. 38, No. 9, pp. 1814-1822, 20 March 1999.

9. K. Komurasaki, M. Sugimine, S. Hosoda, Y. Arakawa: "Laser Absorption Measurement of Atomic Oxygen in Arc-Heater Plumes", Paper AIAA-2001-0814, Aerospace Sciences Meeting and Exhibit, 39th, Reno, NV, Jan. 8-11, 2001.

10. G. Herdrich, M. Auweter-Kurtz, H. Kurtz, T. Laux, E. Schreiber: "Investigation of the Inductively Heated Plasmagenerator IPG3 using Injection Rings of Different Geometries", AIAA-2000-2445, 21st Advanced Measurement Technology and Ground Testing Conference, Denver, CO, June 2000.

11. L. Maraffa, A. Smith, A. Santovincenzo, R. Rouméas, J.-P. Huot, G. Scoon, "Aerothermo-dynamics Aspects of Venus Sample Return Mission", 3rd European Symposium on Aerothermodynamics for Space Vehicles, ESTEC, Noordwijk, The Nether-lands, ESA-SP 426, 24th-26th November 1998.

12. V. Rubio Garcia, L. Maraffa, G. Scoon, R. Rouméas, R. Seiler, "Mars Mini-Probes. Elements of Aerothermodynamics and Entry Trajectories", 3rd European Symposium on Aerothermodynamics for Space Vehicles, ESTEC, Noordwijk, The Nether-lands, ESA-SP 426, 24th-26th November 1998.

13. W. O'Neil, Ch. Cazeau, "The Mars Sample Return Mission", IAF-99-Q.3.02, 50th International Astronautical Congress, Amsterdam, The Netherlands, Oct 1999.

14. F. Vilbig, "Lehrbuch der Hochfrequenztechnik", Vol. 2,

Akademische Verlagsges. m. b. H., Frankfurt am Main 1958.

15. Technical Specification of the rf-capacitors and the Triode RS 3300 CJ of the PWK3-IPG energy supply, Fritz Düsseldorf Ges. m. b. H., 1997.

16. G. Herdrich, M. Auweter-Kurtz, H. Kurtz: A New Inductively Heated Plasma Source for Re-Entry Simulations, AIAA-98-3022, 20th AIAA Advance Measurement and Ground Testing Conference, Albuquerque, NM, Juni 1998.

17. PEARSON

18. Mellon, M. G.: Analytical absorption spectroscopy (absrptimetry and colorimetry), John Willey &Sons, Inc., New York, pp. 78-98.

19. Zel'dovich, Y. B., Raizer, Y. P., Hayes, W. D. And Probstain, R. F.: Physics of shock waves and high-temperature hydrodynamic phenomena, Academic Press New York (1966), pp. 107-172.

20. Lochte-Holtgreven W.: Plasma Diagnostics, Norty-Holland Publishing Company, Amsterdam (1968), pp. 9-65.

21. Bear, D. S., Chang, H. A. and Hanson, R. K.: Semiconductor laser absorption diagnostics of atomic oxygen for atmospheric-pressure plasmas, AIAA paper 98-0822, 1998.